 

# Photoinduced Charge-Separation and Charge-Recombination Processes of Oligo(thienyleneethynyl)–Fullerene Dyad Molecules

**Mamoru Fujitsuka,[1,†] Takashi Makinoshima,[1] Atushi Takamizawa,[1] Yasuyuki Araki,[1] Osamu Ito,*[1] Yuko Obara,[2] Yoshio Aso,[2,†] and Tetsuo Otsubo*[2]**

[1]Institute of Multidisciplinary Research for Advanced Materials, Tohoku University, Katahira, Aoba-ku, Sendai 980-8577

[2]Department of Applied Chemistry, Faculty of Engineering, Hiroshima University, Higashi-hiroshima 739-8527

Received January 13, 2006; E-mail: ito@tagen.tohoku.ac.jp

Photoinduced charge-separation and -recombination processes in two series of oligo(thienyleneethynyl)–fullerene dyads (abbreviated as *n*TE–$C_{60}$), in which the *n*TE moiety has a linear (*n*$\alpha$TE) or zigzag structure (*n*$\beta$TE), have been investigated by using transient absorption spectroscopy with sub-picosecond laser flash photolysis. Based on the transient absorption spectra, charge separation occurs in *n*TE–$C_{60}$ with the rate constants on the order of $10^{11}$ $s^{-1}$, indicating almost quantitative charge separation. For all *n*TE–$C_{60}$ dyads, the charge-separation rate-constants in toluene were larger than those in benzonitrile, suggesting that the charge-separation process is a solvent-controlled adiabatic process. On the other hand, the charge-recombination processes going back to the ground state occurred with the rate constants on the order of $10^8$–$10^9$ $s^{-1}$. The charge-recombination rate of *n*$\alpha$TE–$C_{60}$ was faster than that in *n*$\beta$TE–$C_{60}$ with a zigzag structure, in spite of similar free energy change for the charge recombination.

Recently, photoinduced charge-separation and -recombination processes of fullerene molecules linked with an electron-donor molecule via a covalent bond have been extensively investigated by several groups.[1–52] For fullerene molecules linked with a donor, fast charge-separation and slow charge-recombination processes have been reported.[9] As for donors of the dyad molecules including $C_{60}$, aromatic amino compounds,[3–5] carotenoid,[6] porphyrins,[7–15] tetrathiafulvalenes,[16–19] and oligothiophenes[20–31] have been employed. Some of the fullerene–donor linked molecules on an electrode exhibited excellent photovoltaic effects upon photo-irradiation.[10,22] These interesting properties can be attributed to high efficiency of the charge-separation process and stability of the charge-separated states in the fullerene–donor linked molecules.[32–43]

Oligomers of $\pi$-conjugated polymers, such as oligothiophenes, are good electron donors in the ground and excited states. It has been showed that the photoinduced charge-separation processes occurred almost quantitatively in the dyad molecules of oligothiophene and $C_{60}$, in which the charge-separated states have long lifetimes in microsecond region.[20,21,25] Photocurrent generation in the photovoltaic cell including a gold electrode modified with oligothiohene–$C_{60}$ dyad was also demonstrated by Hirayama et al.[22] Photoinduced charge-separation processes in the dyad and triad composed with oligothiophene and $C_{60}$ were also indicated by Janssen and his co-workers.[23,24,27–31] Furthermore, Janssen et al. observed the efficient charge-separation processes in the $C_{60}$ dyad molecules involving oligo(thienylenevinyl) as a donor moiety.[44–52]

Recently, we investigated the photoexcited states and electron-transfer properties of two series of oligo(thienyleneethynyl)s, in which thiophene rings were connected with ethynyl groups at the 2,5- or 2,3-positions (*n*$\alpha$TE or *n*$\beta$TE, respectively, Chart 1).[53] These oligomers exhibited moderate donor-ability; they showed photoinduced intermolecular electron transfer to triplet excited states of $C_{60}$ and $C_{70}$.[53] These find-

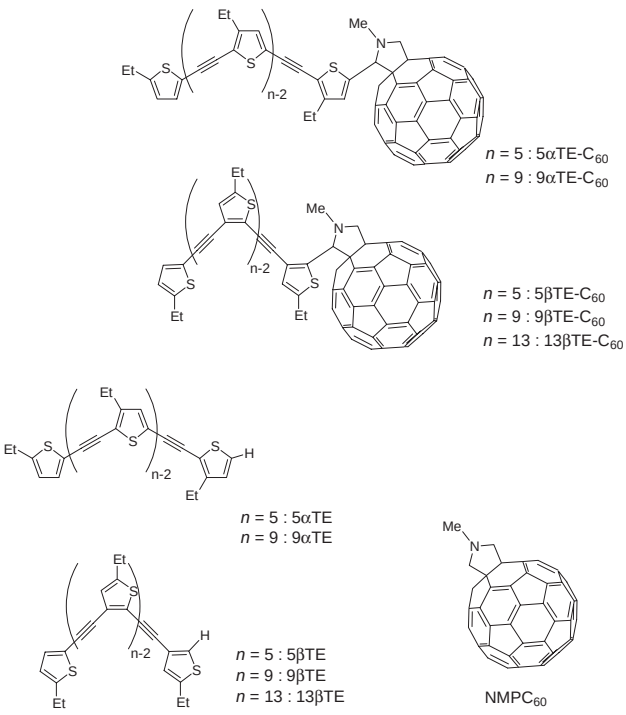


Chart 1.

† Present address: The Institute of Scientific and Industrial Research, Osaka University, Ibaraki, Osaka 567-0047

Published on the web December 13, 2006; doi:10.1246/bcsj.79.1860

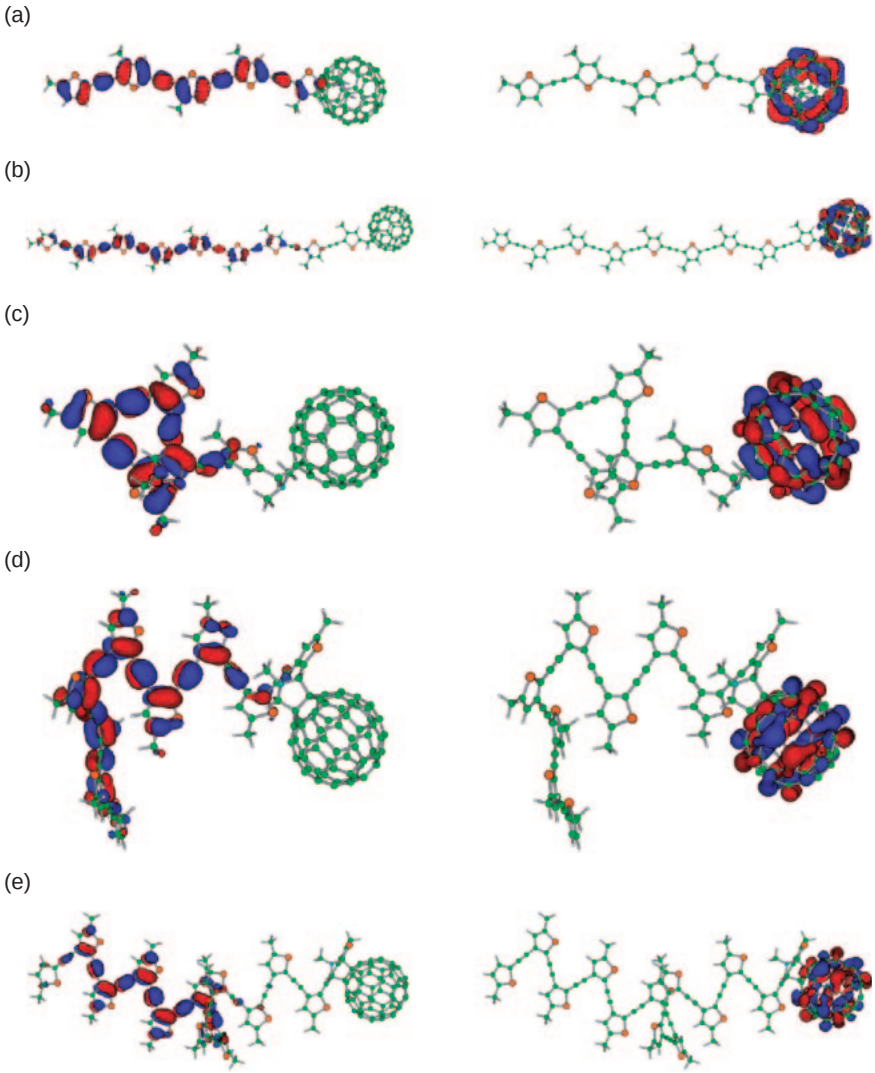


Fig. 1. (Left) HOMO's and (right) LUMO's of (a) 5$\alpha$TE–$C_{60}$, (b) 9$\alpha$TE–$C_{60}$, (c) 5$\beta$TE–$C_{60}$, (d) 9$\beta$TE–$C_{60}$, and (e) 13$\beta$TE–$C_{60}$ calculated at B3LYP/3-21G(d) level.

ings indicate that these oligomers are also candidates for the donor moiety of the dyad molecules including fullerenes. In our previous paper,[54] syntheses and preliminary steady-state fluorescence study of the dyad molecules including $C_{60}$ and oligo(thienyleneethynyl) ($n$TE–$C_{60}$, Chart 1) were reported. In the present paper, by employing sub-picosecond laser flash photolysis, we quantitatively investigated the photoinduced intramolecular charge-separation and charge-recombination processes in $n$TE–$C_{60}$.

## Results and Discussion

**MO Calculations.** Based on B3LYP/3-21G(d) level calculations,[55] the $n\alpha$TE moieties of 5$\alpha$TE–$C_{60}$ and 9$\alpha$TE–$C_{60}$ have linear structures, which are favorable for the extension of $\pi$-conjugated systems (Fig. 1). Actually, the HOMO of 5$\alpha$TE–$C_{60}$ is expanded over the whole 5$\alpha$TE moiety. As for 9$\alpha$TE–$C_{60}$, the HOMO is delocalized over the central 6–7 repeating units of the 9$\alpha$TE. The limited delocalization on the 9$\alpha$TE moiety will be related to a general tendency; that is, various properties of the oligomers, such as absorption and fluorescence peaks, showed saturation behavior around six or seven repeating units, although these properties show a substantial dependence on the chain lengths up to hexamer or heptamer.[25] On the other hand, the LUMO is delocalized over the $C_{60}$-moiety for the dyads. It should be stressed that a linear structure of $n\alpha$TE makes the interaction between $n\alpha$TE moiety and $C_{60}$ moiety weak, because spatial interaction is effectively inhibited by the pyrrolidine ring.

In the cases of $n\beta$TE–$C_{60}$, on the other hand, the optimized structures have zigzag oligomer moieties with a unit of two thiophenes connected by an acetylene bond. Since the planar entities are connected by one or two repeating units, $\pi$-conjugation in the oligomer moieties is limited to the planar entities. Accordingly, the HOMOs of the $n\beta$TE moieties are localized on one planar unit as clearly seen with 13$\beta$TE–$C_{60}$. On the other hand, the LUMO is delocalized over the $C_{60}$-moiety for all the dyads. Thus, although charge-separation processes from the $n$TE moiety to the $C_{60}$ moiety are expected upon photoexcitation of the $n$TE–$C_{60}$ dyads, the character of the radical cation on the $n\beta$TE moiety may be quite different from that of the $n\alpha$TE moiety.

**Ground State Properties of $n$TE–$C_{60}$.** Steady-state

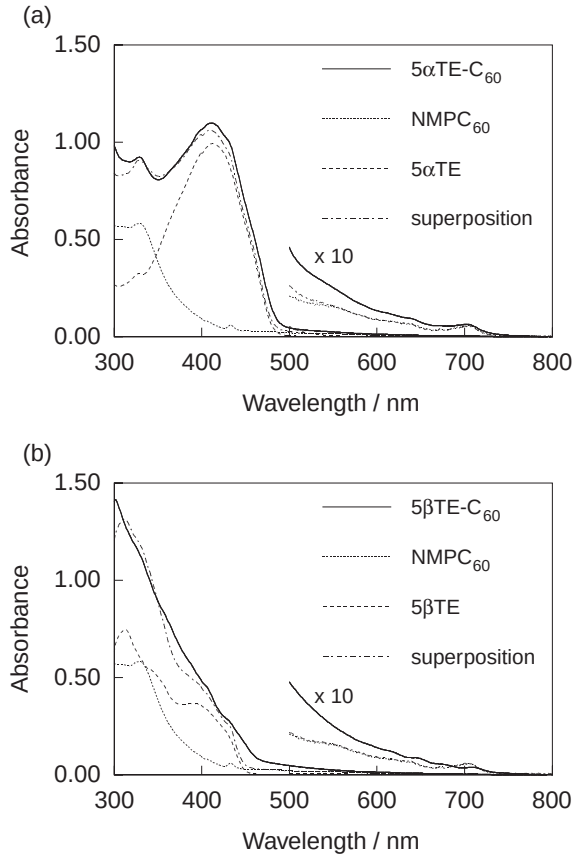


Fig. 2. Absorption spectra of (a) 5$\alpha$TE–$C_{60}$ and (b) 5$\beta$TE–$C_{60}$ in benzonitrile ($1.5 \times 10^{-5}$ M) as well as those of the components.

absorption spectrum of 5$\alpha$TE–$C_{60}$ is shown in Fig. 2a as well as those of 5$\alpha$TE and $NMPC_{60}$, which are the components of the 5$\alpha$TE–$C_{60}$ dyad. In the spectrum of 5$\alpha$TE–$C_{60}$, there were absorption bands at 702, 410, and 330 nm with a shoulder around 435 nm. These absorption bands can be interpreted by superposing the spectra of the components. The absorption bands at 702, 435, and 330 nm are thus attributed to the $C_{60}$ moiety, while the band at 410 nm is assigned to the 5$\alpha$TE-moiety. Since the spectrum of 5$\alpha$TE–$C_{60}$ is essentially the same as the superposition of the components, interaction between the 5$\alpha$TE moiety and the $C_{60}$ moiety seems to be weak in the 5$\alpha$TE–$C_{60}$ dyad. Similarly, weak interaction between the 9$\alpha$TE moiety and the $C_{60}$ moieties was confirmed in an absorption spectrum of 9$\alpha$TE–$C_{60}$, in which the main peak of the 9$\alpha$TE moiety appeared at 450 nm and is red shifted ca. 40 nm from that of 5$\alpha$TE.

On the other hand, the absorption spectrum of 5$\beta$TE–$C_{60}$ (Fig. 2b) does not show a clear peak, because the peak of the 5$\beta$TE-moiety at 310 nm overlaps with that of the $C_{60}$-moiety at 320 nm. The absorption spectrum of 5$\beta$TE–$C_{60}$ cannot be reproduced by the superposition of spectra of the components: (i) in the 300–400 nm region the absorption spectrum of 5$\beta$TE–$C_{60}$ is structure-less compared to the spectral superposition of the components and (ii) the absorption band around 700 nm of 5$\beta$TE–$C_{60}$ is red shifted by 9 nm. Similar spectral features were also confirmed for the absorption spectra of 9$\beta$TE–$C_{60}$ and 13$\beta$TE–$C_{60}$. These findings indicate that the interaction between the $n\beta$TE moiety and the $C_{60}$ moiety is not negligible in $n\beta$TE–$C_{60}$. These features of $n\beta$TE–$C_{60}$ can be attributed to the zigzag structure of $n\beta$TE-moiety, which takes various conformations by rotation around the pyrrolidine–thiophene bond; some of these conformations will induce interaction between the $n\beta$TE- and $C_{60}$-moieties due to their close proximity between the $n\beta$TE- and the $C_{60}$-moieties. On the other hand, $n\alpha$TE–$C_{60}$ showed quite weak interaction due to the linear structures of the $n\alpha$TE moiety normal to the $C_{60}$ sphere as indicated by the MO calculation (Fig. 1).

Table 1. Oxidation ($E_{ox}$) and Reduction Potentials ($E_{red}$) of $n$TE–$C_{60}$ and Related Compounds[a)]

| $n$TE–$C_{60}$ | $E$/V vs $Ag/Ag^+$ | |
|---|---|---|
| | $E_{ox}(n\text{TE}^{+1/0})$ | $E_{red}(C_{60}{}^{0/-1})$ |
| 5$\alpha$TE–$C_{60}$ | 0.86 | −0.88 |
| 9$\alpha$TE–$C_{60}$ | 0.77 | −0.88 |
| 5$\beta$TE–$C_{60}$ | 0.86 | −0.91 |
| 9$\beta$TE–$C_{60}$ | 0.72 | −0.91 |
| 13$\beta$TE–$C_{60}$ | 0.69 | −0.91 |

a) The values were estimated in deaerated benzonitrile containing 0.1 M of tetrabutylammonium perchlorate. $E_{ox}(5\alpha\text{TE}) = 0.88$ V, $E_{ox}(9\alpha\text{TE}) = 0.74$ V, $E_{ox}(5\beta\text{TE}) = 0.84$ V, $E_{ox}(9\beta\text{TE}) = 0.72$ V, $E_{ox}(13\beta\text{TE}) = 0.69$ V, and $E_{red}(\text{NMPC}_{60}) = -0.90$ V.

**Electrochemical Measurements.** Oxidation and reduction potentials of the dyads measured by cyclic voltammetry are summarized in Table 1. The oxidation potentials ($E_{ox}$) of the $n$TE moieties of the $n$TE–$C_{60}$ dyads are essentially the same as those of corresponding $n$TE molecules. In both $n\alpha$TE–$C_{60}$ and $n\beta$TE–$C_{60}$, the $E_{ox}$ values of the $n$TE moieties became less positive with an increase in $n$, which suggests that the $\pi$-conjugation along $n\alpha$TE and $n\beta$TE increases with $n$. The differences in the observed $E_{ox}$ values of the $n$TE moieties seem to be due to the delocalization length of the HOMO in Fig. 1. As for the reduction potentials ($E_{red}$) of the fullerene moieties, the deviations from $NMPC_{60}$ were quite small (<0.02 V). These finings indicate that the interaction between the chromophores of the $n$TE–$C_{60}$ dyads is not so strong as in the ground states. Based on the estimated redox potentials, free energy changes for the charge-separation and -recombination processes ($\Delta G_{CS}$ and $\Delta G_{CR}$, respectively) were calculated employing the Weller equation (Eqs. 1–3):[56]

$$-\Delta G_{CS} = \Delta E_{0\text{–}0} - (-\Delta G_{CR}), \quad (1)$$

$$-\Delta G_{CR} = E_{ox} - E_{red} + \Delta G_S, \quad (2)$$

$$\Delta G_S = e^2/(4\pi\varepsilon_0)[(1/(2r_+) + 1/(2r_-) - 1/R_{cc}) \times (1/\varepsilon_s) - (1/(2r_+) + 1/(2r_-))(1/\varepsilon_r)], \quad (3)$$

where $\Delta E_{0\text{–}0}$ is excitation energy, $r_+$ and $r_-$ are ionic radii of donor and acceptor, respectively, $R_{cc}$ is center-to-center distance, and $\varepsilon_s$ are $\varepsilon_r$ are dielectric constants of solvent for the rate measurements and redox measurements, respectively. Estimated driving force values are summarized in Tables 2 and 3. Geometrical parameters employed are summarized in the footnote of Table 2. As indicated above, we employed the center-to-center distance to calculate $\Delta G_{CS}$ and $\Delta G_{CR}$. This treatment seems to be adequate for the $n\alpha$TE–$C_{60}$, because the LUMO of $n\alpha$TE is delocalized over the central part

Table 2. Free-Energy Changes ($\Delta G_{CS}$), Rate Constants ($k_{CS}$), and Quantum Yields ($\Phi_{CS}$) for Charge-Separation Processes of $n$TE–$C_{60}$ Dyads in Benzonitrile and Toluene

| Dyad | Solvent | $-\Delta G_{CS}$/eV[a)] | $k_{CS}/s^{-1}$ | $\Phi_{CS}$ |
|---|---|---|---|---|
| 5αTE–$C_{60}$ | benzonitrile | 0.93 | $1.2 \times 10^{11}$ | 0.97 |
| | toluene | 0.47 | $3.6 \times 10^{11}$ | 0.97 |
| 9αTE–$C_{60}$ | benzonitrile | 0.80 | $2.8 \times 10^{11}$ | 0.97 |
| | toluene | 0.38 | $4.0 \times 10^{11}$ | 0.97 |
| 5βTE–$C_{60}$ | benzonitrile | 1.02 | $1.4 \times 10^{11}$ | 0.99 |
| | toluene | 0.56 | $4.9 \times 10^{11}$ | 0.99 |
| 9βTE–$C_{60}$ | benzonitrile | 0.98 | $1.1 \times 10^{11}$ | 0.98 |
| | toluene | 0.52 | $2.8 \times 10^{11}$ | 0.98 |
| 13βTE–$C_{60}$ | benzonitrile | 0.94 | $1.5 \times 10^{11}$ | 0.98 |
| | toluene | 0.50 | $3.9 \times 10^{11}$ | 0.97 |

a) $\Delta G_{CS}$ values were calculated assuming that the radii of $C_{60}$, 5αTE, 9αTE, 5βTE, 9βTE, and 13βTE are to be 4.2, 13.4, 24.0, 8.8, 14.7, and 20.6 Å, respectively. The center to center distances are 16.8, 26.5, 11.0, 15.7, and 23.0 Å for 5αTE–$C_{60}$, 9αTE–$C_{60}$, 5βTE–$C_{60}$, 9βTE–$C_{60}$, and 13βTE–$C_{60}$, respectively. The respective singlet energies were 2.61, 2.50, 2.81, 2.64, and 2.56 eV.

Table 3. Free-Energy Changes ($\Delta G_{CR}$), Rate Constants ($k_{CR}$) for Charge-Recombination Process, and Lifetimes of Radical Ion Pair ($\tau_{ion}$) of $n$TE–$C_{60}$ Dyads in Benzonitrile and Toluene

| Dyad | Solvent | $-\Delta G_{CR}$/eV[a)] | $k_{CR}/s^{-1}$ | $\tau_{ion}$/ns |
|---|---|---|---|---|
| 5αTE–$C_{60}$ | benzonitrile | 1.78 | $3.6 \times 10^{9}$ | 0.28 |
| | toluene | 2.24 | $2.6 \times 10^{9}$ | 0.38 |
| 9αTE–$C_{60}$ | benzonitrile | 1.70 | $6.2 \times 10^{9}$ | 0.16 |
| | toluene | 2.12 | $5.9 \times 10^{9}$ | 0.17 |
| 5βTE–$C_{60}$ | benzonitrile | 1.79 | $2.9 \times 10^{8}$ | 3.4 |
| | toluene | 2.25 | $2.6 \times 10^{8}$ | 3.8 |
| 9βTE–$C_{60}$ | benzonitrile | 1.66 | $2.5 \times 10^{8}$ | 4.0 |
| | toluene | 2.12 | $1.2 \times 10^{8}$ | 8.3 |
| 13βTE–$C_{60}$ | benzonitrile | 1.62 | $3.4 \times 10^{8}$ | 2.9 |
| | toluene | 2.04 | $1.6 \times 10^{8}$ | 6.3 |

a) $\Delta G_{CR}$ values were calculated employing the parameters listed in the caption of Table 2.

of $n$αTE moiety. In the case of $n$βTE–$C_{60}$, the LUMO of $n$βTE is localized on a planar entity of the $n$βTE. Furthermore, the zigzag structure of $n$βTE allows various conformers. Thus, the estimated $\Delta G_{CS}$ and $\Delta G_{CR}$ values for $n$βTE–$C_{60}$ (Tables 2 and 3) should be regarded as a typical value. By assuming that the LUMO of 13βTE is localized on a planar entity of $n$βTE close to $C_{60}$, a $\Delta G_{CS}$ value of $-0.98$ eV is expected in benzonitrile. On the other hand, a $\Delta G_{CS}$ value of $-0.93$ eV is expected when the LUMO of 13βTE is localized on the other end of the $n$βTE chain. A similar variation in $\Delta G_{CS}$ is expected for other $n$βTE–$C_{60}$ dyads. As a whole, the charge-separation processes from the excited $n$TE moiety in the $n$TE–$C_{60}$ dyads are exothermic in benzonitrile as indicated in a schematic energy diagram (Fig. 3). Even in nonpolar toluene, negative $\Delta G_{CS}$ values were calculated, although a large error may be included. On the other hand, the $\Delta G_{CS}$ values via the excited singlet state of the $C_{60}$ moiety, which can be calculated employing $\Delta E_{0\text{–}0} = 1.74$ eV and $\Delta G_{CR}$ in Table 3, are only slightly negative in benzonitrile and positive in toluene.

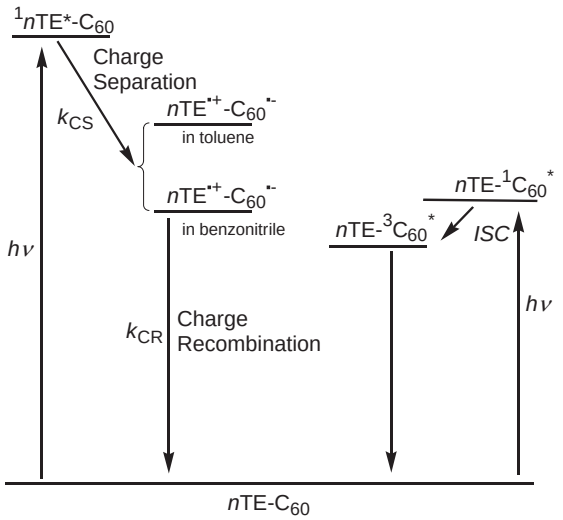


Fig. 3. Schematic energy diagram for the photoinduced processes of $n$TE–$C_{60}$.

**Fluorescence Properties of $n$TE–$C_{60}$.** Fluorescence spectra of the $n$TE–$C_{60}$ dyads in toluene were estimated for the $n$TE moiety and the $C_{60}$ moiety separately as shown in Fig. 4. Note that the spectra in the regions of 400–650 and 670–850 nm were measured with different sample concentrations in order to make clear the contribution of each excited state to the photoinduced process, such as charge separation. For the spectra in the 400–650 nm region, the concentrations of the samples were adjusted so that the same number of photons is absorbed by the $n$TE-moiety. In the 450–650 nm region, fluorescence intensities of the $n$TE moieties of the $n$TE–$C_{60}$ dyads are quite low when compared to the corresponding $n$TE references. For example, fluorescence intensity of the 5αTE moiety of 5αTE–$C_{60}$ is 1/10000 of 5αTE. This finding indicates that a photoinduced process, such as charge transfer, occurs in $n$TE–$C_{60}$ via the singlet excited states of the $n$TE moieties ($^1n$TE*) of the $n$TE–$C_{60}$ dyads. As for the fluorescence spectra in the 670–850 nm region, the fluorescence intensities of the $C_{60}$ moiety of $n$TE–$C_{60}$ are similar to that of NMP$C_{60}$, even after careful adjustment of the concentration of the sample so that the same number of photons is absorbed by $C_{60}$ moiety. These observations indicate that both new deactivation process via the singlet excited state of the $C_{60}$ moiety ($^1C_{60}$*) and energy transfer from $^1n$TE* to the $C_{60}$ moiety are not included.

Fluorescence spectra were also measured in polar solvents, such as benzonitrile. Extensive fluorescence quenching of the $n$TE moieties was also confirmed for the $n$TE–$C_{60}$ dyads. Similar to the observation in toluene, the $C_{60}$ moiety of $n$TE–$C_{60}$ did not show any appreciable change in the fluorescence intensities compared with that of NMP$C_{60}$ even after the sample concentrations were adjusted so that the same number of the photons was absorbed by the $C_{60}$ moiety.

These findings do not support an energy-transfer process from the $^1n$TE* moiety to the $C_{60}$ moiety in both solvents, since no increase in the fluorescence intensity resulting from the accumulation of $^1C_{60}$* by the energy transfer from $^1n$TE* was observed.

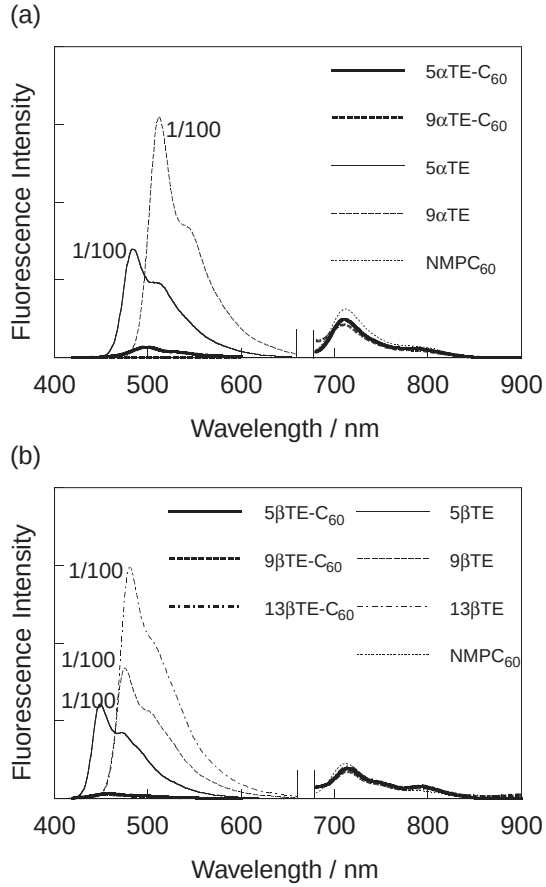


Fig. 4. Fluorescence spectra of (a) 5$\alpha$TE–$C_{60}$ and 9$\alpha$TE–$C_{60}$ and (b) 5$\beta$TE–$C_{60}$, 9$\beta$TE–$C_{60}$, and 13$\beta$TE–$C_{60}$ with the components of the dyads in toluene upon excitation at 400 nm. Concentrations of samples were adjusted so that the same number of photons is absorbed by the corresponding chromophores.

The fluorescence lifetimes of the *n*TE moieties of *n*TE–$C_{60}$ were shorter than our instrumental limit (<20 ps) in toluene and in benzonitrile, indicating that a fast photoinduced process occurs via the $^1$*n*TE* moieties of the *n*TE–$C_{60}$ dyads. This observation is quite reasonable, because the energy of $^1$*n*TE* is high enough to cause photoinduced charge separation even in toluene. As for the $C_{60}$ moieties in *n*TE–$C_{60}$, the lifetimes were 1.1–1.2 ns, which are almost the same as that of $NMPC_{60}$,[57] indicating the absence of a fast deactivation process in the $^1C_{60}$* moieties. The absence of the fast deactivation process, such as charge separation, is quite reasonable, since the driving force for the charge separation from the $^1C_{60}$* moiety of the *n*TE–$C_{60}$ dyad in toluene is endothermic (Fig. 3).

**Transient Absorption Spectra of *n*TE–$C_{60}$.** In order to study the processes involving the singlet excited states of the *n*TE–$C_{60}$ dyads in detail, sub-picosecond transient absorption spectra were measured by exciting samples with 388 nm laser light from a femtosecond laser (fwhm 150 fs). In Fig. 5, transient absorption spectra of 9$\beta$TE–$C_{60}$ in benzonitrile are shown as a representative case. An absorption band appeared in the 470–600 nm region with an absorption tailing to wavelengths longer than 900 nm immediately after laser irradiation. The spectrum at 2 ps can be attributed mainly to the $^1$9$\beta$TE* moiety from the comparison with the spectrum previously reported for $^1$9$\beta$TE*.[53] Contribution of the $^1C_{60}$* moiety should be minor in the present case, because the characteristic absorption band due to the $^1C_{60}$* moiety around 900 nm is not clear in the spectrum.[58] This finding agrees with the fact that ca. 3/4 of photons of the 388 nm laser light are absorbed by the 9$\beta$TE-moiety of the dyad. At 40 ps after laser irradiation, a new absorption band appeared around 560 nm with an increasing absorption-time profile as shown in the 0–40 ps time region in Fig. 5b. The absorption band around 560 nm can be attributed to the radical cation of the 9$\beta$TE moiety (9$\beta$TE$^{\bullet+}$), which showed the absorption peak at 688 nm during $\gamma$-ray radiolysis in 77 K glassy matrix.[53] The absorption peak shift of 9$\beta$TE$^{\bullet+}$ between the 77 K glassy matrix and solution at room temperature can be attributed to structural relaxation that is dependent on the temperature change, because *n*$\beta$TE tends to take more

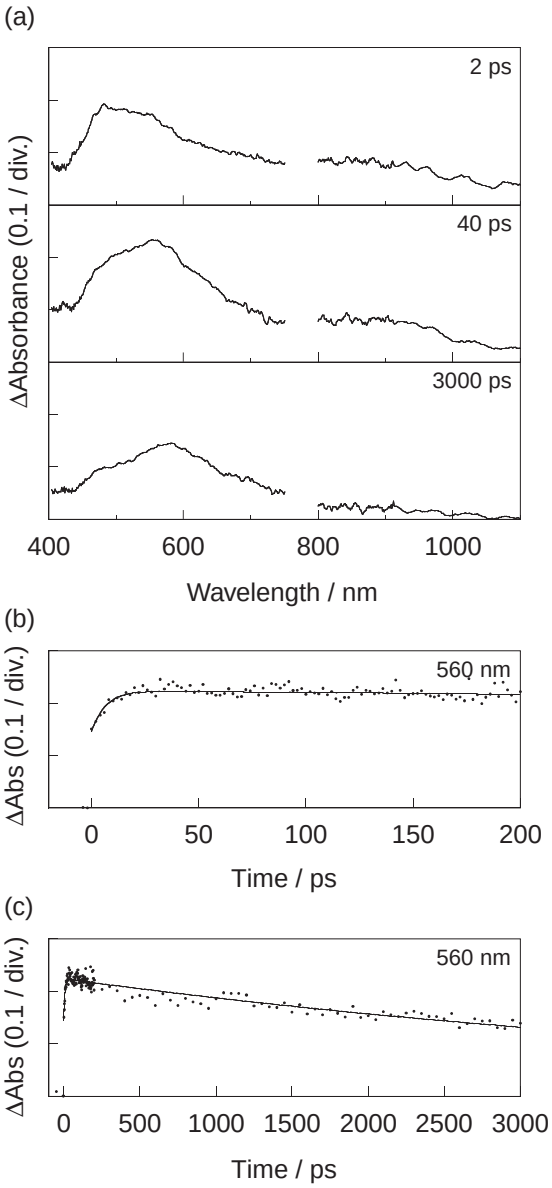


Fig. 5. (a) Transient absorption spectra of 9$\beta$TE–$C_{60}$ in benzonitrile upon excitation with 388 nm laser light (fwhm 150 fs), (b) and (c) absorption-time profiles at 560 nm.

planar structure at lower temperatures, which is well known for various conjugated polymers.[59] Accordingly, a shoulder around 980 nm is attributable to the radical anion of functionalized $C_{60}$ ($C_{60}^{\bullet-}$).[60] This fact indicates that charge separation occurred from the $^1 9\beta$TE* moiety to the $C_{60}$ moiety in benzonitrile. For other $n\beta$TE–$C_{60}$, similar transient absorption spectra were observed indicating the charge-separation process as shown in Eq. 4:

$$n\beta\text{TE–C}_{60} \xrightarrow{h\nu(388\,\text{nm})} {}^1 n\beta\text{TE}^*\text{–C}_{60} \xrightarrow[(n=5,9,13)]{k_{CS}} n\beta\text{TE}^{\bullet+}\text{–C}_{60}^{\bullet-}, \quad (4)$$

where $k_{CS}$ denotes a rate constant for the charge separation of $^1 n\beta$TE*–$C_{60}$. In toluene, the appearances of the $n\beta\text{TE}^{\bullet+}$ moieties in $n\beta$TE–$C_{60}$ were confirmed in almost the same time region (ca. 40 ps), supporting the charge-separation process, Eq. 4. The timescale for the generation of $n\beta\text{TE}^{\bullet+}\text{–C}_{60}^{\bullet-}$ (<10 ps) agrees with the lifetime of the fluorescence of the $n\beta$TE moiety of $n\beta$TE–$C_{60}$ being less than 20 ps in toluene and benzonitrile.

Contribution of the $^1C_{60}$* moiety to the charge-separation process can be neglected, since the fluorescence lifetime of the $C_{60}$ moiety (1.2 ns) was quite longer than the timescale for the generation of $n\beta\text{TE}^{\bullet+}\text{–C}_{60}^{\bullet-}$ (<10 ps), which correlates to the lifetime of the fluorescence of the $n\beta$TE moiety. Because there is no contribution from the $^1C_{60}$* moiety in the charge-separation process, the main deactivation pathway of the $^1 n\beta$TE* moiety is charge separation but not energy transfer. This is consistent with the fact that the $^1C_{60}$* moiety cannot access the charge-separated state especially in nonpolar solvents (vide infra).

Assuming that the generation of $9\beta\text{TE}^{\bullet+}\text{–C}_{60}^{\bullet-}$ and the decay of the $^1 9\beta$TE* moiety are included in the absorption-time profile of Fig. 4b, the $k_{CS}$ value was estimated to be $1.1 \times 10^{11}$ $s^{-1}$ in benzonitrile by using curve-fitting method. Similarly, the $k_{CS}$ values were evaluated for other $n\beta$TE–$C_{60}$ in benzonitrile and toluene as listed in Table 2. Large $k_{CS}$ values indicate almost quantitative generation of the charge-separated state from the $^1 n\beta$TE* moiety as shown in a schematic energy diagram (Fig. 3). The quantum yields for the charge separation ($\Phi_{CS}$) were estimated to be 0.97–0.99 from the relation $\Phi_{CS} = k_{CS}/(k_{CS} + k_S)$, where $k_S$ is a singlet decay rate of the $n\beta$TE moiety estimated from the fluorescence lifetime of the $n\beta$TE model. Negligible contribution of the $^1C_{60}$* moiety is attributed to the higher energy levels of the charge-separated states than the $^1C_{60}$* moiety for all $n\beta$TE–$C_{60}$ in toluene. In benzonitrile, even for $9\beta$TE–$C_{60}$ and $13\beta$TE–$C_{60}$, the energy levels of the charge-separated states are similar to the energy level of the $^1C_{60}$* moiety as evaluated from the $\Delta G_{CR}$ values in Table 3, indicating a negligible charge-separation process.

The photoinduced processes of the $n\alpha$TE–$C_{60}$ dyad molecules were also investigated with sub-picosecond laser flash photolysis. In the case of $9\alpha$TE–$C_{60}$ in benzonitrile, generation of the $^1 9\alpha$TE* moiety was confirmed by observation of an absorption band in the near-IR region (800–1100 nm) as shown in Fig. 6a.[53] The $^1 9\alpha$TE* moiety decayed within 20 ps as shown in Fig. 6b, leaving the absorption bands around 740 and 520 nm in the spectrum at 40 ps, which can be attributed to the $9\alpha\text{TE}^{\bullet+}$ moiety,[53] indicating that the charge-separation

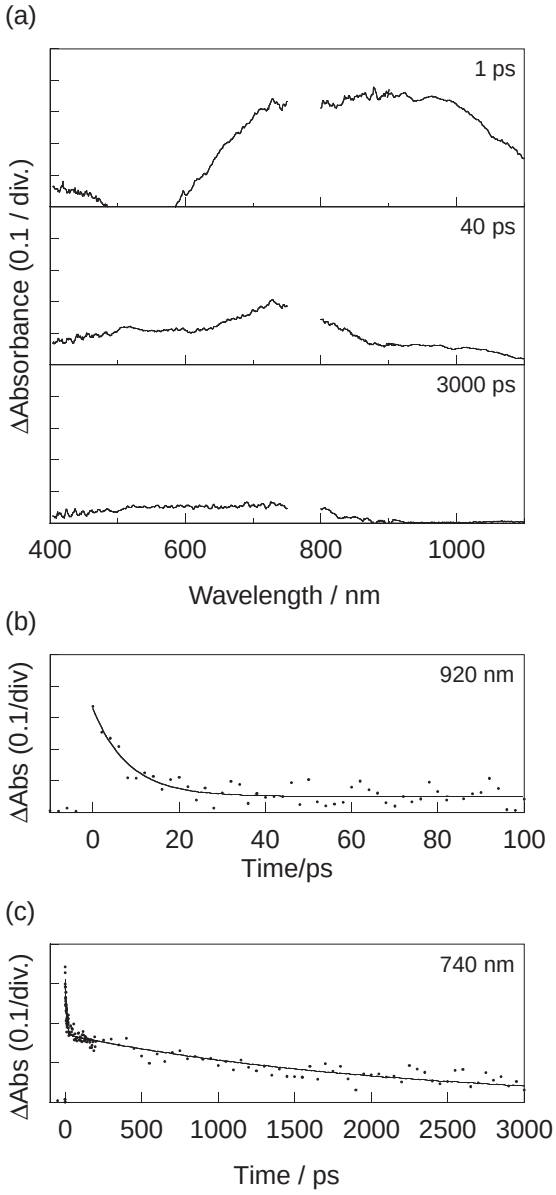


Fig. 6. (a) Transient absorption spectra of $9\alpha$TE–$C_{60}$ in benzonitrile upon excitation with 388 nm laser light (fwhm 150 fs), (b) and (c) absorption-time profiles at 920 and 740 nm, respectively.

process takes place via the $^1 9\alpha$TE* moiety, Eq. 5, in a similar manner to the process in Eq. 4.

$$n\alpha\text{TE–C}_{60} \xrightarrow{h\nu(388\,\text{nm})} {}^1 n\alpha\text{TE}^*\text{–C}_{60} \xrightarrow[(n=5,9)]{k_{CS}} n\alpha\text{TE}^{\bullet+}\text{–C}_{60}^{\bullet-}. \quad (5)$$

The absorption peak of the $C_{60}^{\bullet-}$ moiety appeared in the 900–1000 nm region, which seems to be overlapped with an absorption tail of the band for the $9\alpha\text{TE}^{\bullet+}$ moiety at 740 nm. The $k_{CS}$ value was estimated to be $2.8 \times 10^{11}$ $s^{-1}$ from the decay curve of the $^1 9\alpha$TE* moiety in Fig. 6b. In the case of $9\alpha$TE–$C_{60}$, the contribution of the singlet excited state of the $C_{60}$ moiety can be also neglected, because a sufficiently large $-\Delta G_{CS}$ cannot be expected from energetic consideration even

in benzonitrile. For 5$\alpha$TE–$C_{60}$, the charge-separation process from the $^1$5$\alpha$TE* moiety was also confirmed. Furthermore, the charge-separation process was also confirmed in non-polar toluene solvent.

The $k_{CS}$ values as well as the $\Delta G_{CS}$ values are summarized in Table 2. Both in benzonitrile and toluene, $k_{CS}$ is quite large. One of the reasons for the fast charge separation can be attributed to a process near the Marcus top region.[61–63] The solvent reorganization energy ($\lambda_s$) in the present charge-transfer system can be estimated using the structural parameters listed in the footnote of Table 2 and following Eq. 6,

$$\lambda_S = e^2/(4\pi\varepsilon_0)[(1/(2r_+) + 1/(2r_-) - 1/R_{cc}) \times (1/\varepsilon_{op} - 1/\varepsilon_S)], \quad (6)$$

where $\varepsilon_{op}$ is the dielectric constant for the optical region. For dyads in benzonitrile and toluene, the $\lambda_S$ value was estimated to be 0.39–0.57 and 0.26–0.38 eV, respectively. Since the internal reorganization energy for the donor–fullerene dyad was reported to be $\approx$0.3 eV,[4] total reorganization energy is 0.7–0.9 and 0.6–0.7 eV in benzonitrile and toluene, respectively. These values are similar to the $-\Delta G_{CS}$ values listed in Table 2, indicating that the present charge-separation process proceeds with almost no barrier in both solvents.

Since $k_{CS}$ is on the order of $10^{11}$ s$^{-1}$, the electronic coupling matrix element ($V$) is on the order of 10 to 100 cm$^{-1}$. This value seems to be adequate since the Williams et al. reported $V = 28$ cm$^{-1}$ for the covalently bonded dyad including *N*,*N*-dimethylaniline and $C_{60}$.[4] By assuming $V = 50$ cm$^{-1}$ and $\lambda_S = 0.5$ eV, the adiabaticity parameter ($\kappa = 4\pi V^2\tau_l/\hbar\lambda_S$, $\hbar$: Planck's constant, $\tau_l$: longitudinal dielectric relaxation time) is calculated to be 7.3, indicating that the present charge-transfer process proceeds as a solvent-controlled adiabatic reaction.[64] Actually, the observed $k_{CS}$ values ((3.6–9.1 ps)$^{-1}$ and (2.0–3.6 ps)$^{-1}$ in benzonitrile and toluene, respectively) are almost the same as the $\tau_l$ values (5.1 and 2.7 ps in benzonitrile and toluene, respectively).[65,66] Therefore, the faster charge separation in toluene than in benzonitrile can be attributed to fast solvation in toluene. Previously, we reported that, from the steady-state fluorescence, $n\beta$TE seems to expand its $\pi$-conjugation system in the excited state.[53] The larger $\pi$-conjugation causes a larger electronic coupling matrix element in the charge-transfer process, since it makes hopping of excitation energy to the vicinity of the fullerene moiety possible. The solvent-controlled adiabatic reaction and delocalization of the excited state seem to explain the weak dependence of charge-separation rate on the charge-separation distance in the present dyads.

As shown in an absorption-time profile of Fig. 6c, the absorption band due to the radical ion pair shows decay over several nanoseconds. The decay can be attributed to the charge-recombination process (Eq. 7):

$$n\text{TE}^{\bullet+}\text{–}C_{60}^{\bullet-} \xrightarrow{k_{CR}} n\text{TE–}C_{60}, \quad (7)$$

where $k_{CR}$ denotes the rate constant for the charge-recombination process generating the ground state of the dyad as shown in the energy diagram (Fig. 3). The decays of the radical ion pairs over several nanoseconds were also confirmed for other $n\beta$TE–$C_{60}$ dyads molecules as shown in Fig. 5c. The observed $k_{CR}$ values as well as $\Delta G_{CR}$ values are summarized in Table 3. The $k_{CR}$ values are $6.2 \times 10^9$–$1.2 \times 10^8$ s$^{-1}$, indicating that charge-separated states have lifetimes of 0.16–8.3 ns.

The $k_{CR}$ values of $n\beta$TE–$C_{60}$ are smaller than those of $n\alpha$TE–$C_{60}$ even if the $-\Delta G_{CR}$ values are similar. As a reason of the different $k_{CR}$ values between $n\alpha$TE–$C_{60}$ and $n\beta$TE–$C_{60}$, the following possibilities can be pointed out. (1) There is a difference in the internal reorganization energy between $n\alpha$TE–$C_{60}$ and $n\beta$TE–$C_{60}$. A slight change in the reorganization energy can result in a large difference in charge-separation and -recombination rates. (2) Delocalization of hole in the conjugated chain causes the difference in $k_{CR}$ values. In the case of $n\alpha$TE–$C_{60}$, the radical cation is expected to be delocalized over the oligomer chain, while a localized radical cation is expected for $n\beta$TE–$C_{60}$. The delocalized radical cation of $n\alpha$TE–$C_{60}$ is expected to cause fast charge recombination, since the radical ion pair can be recombined at rather close proximity to each other. (3) Difference in the hopping rate of the radical cation along the oligomer chain causes the difference in $k_{CR}$ values. For the oligomer of conjugated polymer, hopping of the radical cation is expected. If the hopping rate is faster than $k_{CR}$ expected from Marcus theory, charge recombination after the hopping of the radical cation becomes important, because due to hopping the radical cation can be in close proximity of the radical anion. Hopping in the linear oligomer chain should effectively increase $k_{CR}$. At the present stage of our study, we cannot evaluate the contribution of each factor. However, the dependence of $k_{CR}$ on molecular structure rather than the driving force is an interesting property of these conjugated oligomers.

## Conclusion

In the present study, we showed that fast charge-separation processes occur in the two series of $n$TE–$C_{60}$ dyads, in which the $n$TE moiety has a linear or a zigzag structure. The $k_{CS}$ values were on the order of $10^{11}$ s$^{-1}$, indicating almost quantitative charge separation. For all dyads, $k_{CS}$ in toluene was larger than that in benzonitrile, because charge-separation is a solvent-controlled adiabatic process. The $k_{CR}$ of the $n\alpha$TE–$C_{60}$ was greater than that of $n\beta$TE–$C_{60}$ reflecting the molecular structure rather than the driving force for the recombination.

## Experimental

**Materials.** Syntheses of $n\alpha$TE, $n\beta$TE, $n\alpha$TE–$C_{60}$, $n\beta$TE–$C_{60}$, and NMP$C_{60}$ in Chart 1 were performed by the methods previously described.[54] Other chemicals were of the best commercial grade available.

**Apparatus.** The sub-picosecond transient absorption spectra were measured by the pump and probe method. The samples were excited with a second harmonic generation (SHG, 388 nm) of output from a femtosecond Ti:sapphire regenerative amplifier seeded by SHG of a Er-doped fiber laser (Clark-MXR CPA-2001 plus, 1 kHz, fwhm 150 fs). The excitation light was depolarized. A white continuum pulse generated by focusing the fundamental light on a $H_2O$ cell was used as a monitoring light. The visible monitoring light transmitted through the sample was detected with a dual MOS detector (Hamamatsu Photonics, C6140) equipped with a polychromator (Acton Research, SpectraPro 150). For the spectra in the near-IR region, InGaAs photodiode array (Hamamatsu Photonics, C5890-128) was employed as the detector. The spectra were obtained by averaging on a microcomputer.[26]

Fluorescence lifetimes were measured by a single photon counting method using a streakscope (Hamamatsu Photonics, C4334-01). The samples were excited with a SHG (410 nm, Spectra-Physics, GWU-23PS) of a Ti:sapphire laser (Spectra-Physics, Tsunami 3950-L2S, fwhm 1.5 ps) pumped by an argon-ion laser (Spectra-Physics, BeamLok 2060-10-SA). Steady-state fluorescence spectra of the samples were measured on a Shimadzu RF-5300PC spectrofluorophotometer.

Steady-state absorption spectra in the visible and near-IR regions were measured on a Jasco V530 spectrophotometer.

Electrochemical measurements were carried out using a BAS CV50W voltammetric analyzer with a three-electrodes system in benzonitrile containing 0.1 M tetrabutylammonium perchlorate. A platinum or glassy carbon electrode was used as the working electrode. A platinum wire served as the counter electrode and a Ag/AgCl was used as the reference electrode. All the solutions were purged prior to electrochemical and spectral measurements using argon gas.

**Molecular Orbital Calculations.** All molecular orbital calculations were performed using the Gaussian 03 package.[55] Geometry optimization and calculations of molecular orbital coefficients were performed using the density functional theory at B3LYP/3-21G(d) level.

The present work was partly supported by a Grant-in-Aid on Scientific Research for Priority Aria (417) from the Ministry of Education, Culture, Sports, Science and Technology of Japan.

## References

1 N. Martín, I. Sánchez, B. Illescas, I. Pérez, *Chem. Rev.* **1998**, *98*, 2527.

2 *Fullerenes*, ed. by K. M. Kadish, R. S. Ruoff, Wiley Interscience, NY, **2000**.

3 R. M. Williams, J. M. Zwier, J. W. Verhoeven, *J. Am. Chem. Soc.* **1995**, *117*, 4093.

4 R. M. Williams, M. Koeberg, J. M. Lawson, Y.-Z. An, Y. Rubin, M. N. Paddon-Row, J. W. Verhoeven, *J. Org. Chem.* **1996**, *61*, 5055.

5 S. Komamine, M. Fujitsuka, O. Ito, K. Moriwaki, T. Miyata, T. Ohno, *J. Phys. Chem. A* **2000**, *104*, 11497.

6 H. Imahori, S. Cardoso, D. Tatman, S. Lin, L. Noss, G. R. Seely, L. Sereno, C. Silber, T. A. Moore, A. L. Moore, D. Gust, *Photochem. Photobiol.* **1995**, *62*, 1009.

7 D. Kuciauskas, S. Lin, G. R. Seely, A. L. Moore, T. A. Moore, D. Gust, T. Drovetskaya, C. A. Reed, P. D. W. Boyd, *J. Phys. Chem.* **1996**, *100*, 15926.

8 H. Imahori, K. Hagiwara, M. Aoki, T. Akiyama, S. Taniguchi, T. Okada, M. Shirakawa, Y. Sakata, *J. Am. Chem. Soc.* **1996**, *118*, 11771.

9 H. Imahori, K. Hagiwara, T. Akiyama, M. Aoki, S. Taniguchi, T. Okada, M. Shirakawa, Y. Sakata, *Chem. Phys. Lett.* **1996**, *263*, 545.

10 H. Imahori, S. Ozawa, K. Uchida, M. Takahashi, T. Azuma, A. Ajavakom, T. Akiyama, M. Hasegawa, S. Taniguchi, T. Okada, Y. Sakata, *Bull. Chem. Soc. Jpn.* **1999**, *72*, 485.

11 N. V. Tkachenko, L. Rantala, A. Y. Tauber, J. Helaja, P. V. Hynninen, H. Lemmetyinen, *J. Am. Chem. Soc.* **1999**, *121*, 9378.

12 D. I. Schuster, P. Cheng, S. R. Wilson, V. Prokhorenko, M. Katterle, A. R. Holzwarth, S. E. Braslavsky, G. Klihm, R. M. Williams, C. Luo, *J. Am. Chem. Soc.* **1999**, *121*, 11599.

13 M. Fujitsuka, O. Ito, H. Imahori, K. Yamada, H. Yamada, Y. Sakata, *Chem. Lett.* **1999**, 721.

14 H. Imahori, K. Tamaki, D. M. Guldi, C. Luo, M. Fujitsuka, O. Ito, Y. Sakata, S. Fukuzumi, *J. Am. Chem. Soc.* **2001**, *123*, 2607.

15 H. Imahori, D. M. Guldi, K. Tamaki, Y. Yoshida, C. Luo, Y. Sakata, S. Fukuzumi, *J. Am. Chem. Soc.* **2001**, *123*, 2607.

16 J. Llacay, J. Veciana, J. Vidal-Gancedo, J. L. Bourdelnde, R. González-Moreno, C. Rovira, *J. Org. Chem.* **1998**, *63*, 5201.

17 N. Martín, L. Sánchez, M. A. Herranz, D. M. Guldi, *J. Phys. Chem. A* **2000**, *104*, 4648.

18 H. Nishikawa, S. Kojima, T. Kodama, I. Ikemoto, S. Suzuki, K. Kikuchi, M. Fujitsuka, H. Luo, Y. Araki, O. Ito, *J. Phys. Chem. A* **2004**, *108*, 1881.

19 L. Sanchez, M. Sierra, N. Martín, D. M. Guldi, M. W. Wienk, R. A. J. Janssen, *Org. Lett.* **2005**, *7*, 1691.

20 T. Yamashiro, Y. Aso, T. Otsubo, H. Tang, T. Harima, K. Yamashita, *Chem. Lett.* **1999**, 443.

21 M. Fujitsuka, O. Ito, T. Yamashiro, Y. Aso, T. Otsubo, *J. Phys. Chem. A* **2000**, *104*, 4876.

22 D. Hirayama, T. Yamashiro, K. Takimiya, Y. Aso, T. Otsubo, H. Norieda, H. Imahori, Y. Sakata, *Chem. Lett.* **2000**, 570.

23 P. A. van Hal, J. Knol, B. M. W. Longeveld-Voss, S. C. J. Meskers, J. C. Hummelen, R. A. J. Janssen, *J. Phys. Chem. A* **2000**, *104*, 5974.

24 J. J. Apperloo, B. M. W. Langeveld-Voss, J. Knol, J. C. Hummelen, R. A. J. Janssen, *Adv. Mater.* **2000**, *12*, 908.

25 M. Fujitsuka, K. Matsumoto, O. Ito, T. Yamashiro, Y. Aso, T. Otsubo, *Res. Chem. Intermed.* **2001**, *27*, 73.

26 M. Fujitsuka, A. Masuhara, H. Kasai, H. Oikawa, H. Nakanishi, O. Ito, T. Yamashiro, Y. Aso, T. Otsubo, *J. Phys. Chem. B* **2001**, *104*, 9930.

27 P. A. van Hal, J. Knol, B. M. W. Langeveld-Voss, S. C. J. Meskers, J. C. Hummelen, R. A. J. Janssen, *Synth. Met.* **2001**, *116*, 123.

28 P. A. van Hal, J. Knol, B. M. W. Langeveld-Voss, S. C. J. Meskers, J. C. Hummelen, R. A. J. Janssen, *Synth. Met.* **2001**, *121*, 1597.

29 P. A. van Hal, R. A. J. Janssen, G. Lanzani, G. Cerullo, M. Zavelani-Rossi, S. De Silvestri, *Chem. Phys. Lett.* **2001**, *345*, 33.

30 P. A. van Hal, E. H. A. Beckers, S. C. J. Meskers, R. A. J. Janssen, B. Jousselme, P. Blanchard, J. Roncali, *Chem. Eur. J.* **2002**, *8*, 5415.

31 E. H. A. Beckers, P. A. van Hal, A. Dhanabalan, S. C. J. Meskers, J. Knol, J. C. Hummelen, R. A. J. Janssen, *J. Phys. Chem. A* **2003**, *107*, 6218.

32 N. S. Sariciftci, F. Wudl, A. J. Heeger, M. Maggini, G. Scorrano, M. Prato, J. Bourassa, P. C. Ford, *Chem. Phys. Lett.* **1995**, *247*, 510.

33 M. Maggini, D. M. Guldi, S. Mondini, G. Scorrano, F. Paolucci, P. Ceroni, S. Roffia, *Chem. Eur. J.* **1998**, *4*, 1992.

34 A. Polese, S. Mondini, A. Bianco, C. Toniolo, G. Scorrano, D. M. Guldi, M. Maggini, *J. Am. Chem. Soc.* **1999**, *121*, 3446.

35 D. M. Guldi, G. T. Garscia, J. Mattay, *J. Phys. Chem. A* **1998**, *102*, 9679.

36 D. M. Guldi, *Chem. Commun.* **2000**, 321.

37 M. Yamazaki, Y. Araki, M. Fujitsuka, O. Ito, *J. Phys. Chem. A* **2001**, *105*, 8615.

38 D. M. Guldi, A. S. Swartz, C. Luo, R. Gómez, J. L. Segura, N. Martín, *J. Am. Chem. Soc.* **2002**, *124*, 10875.

39 M. Fujitsuka, H. Luo, Y. Murata, N. Kato, O. Ito, K. Komatsu, *Chem. Lett.* **2002**, 968.

40 M. Prato, M. Maggini, C. Giacometti, G. Scorrano, G.

Sandonà, G. Farnia, *Tetrahedron* **1996**, *52*, 5221.
41 D. M. Guldi, M. Maggini, G. Scorrano, M. Prato, *J. Am. Chem. Soc.* **1997**, *119*, 974.
42 F. D'Souza, M. E. Zandler, P. M. Smith, G. R. Deviprasad, K. Arkady, M. Fujitsuka, O. Ito, *J. Phys. Chem. A* **2002**, *106*, 649.
43 M. E. Zandler, P. M. Smith, M. Fujitsuka, O. Ito, F. D'Souza, *J. Org. Chem.* **2002**, *67*, 9122.
44 E. Peeters, P. A. van Hal, J. Knol, C. J. Brabec, N. S. Sariciftci, J. C. Hummelen, R. A. J. Janssen, *J. Phys. Chem. B* **2000**, *104*, 10174.
45 P. A. van Hal, E. H. A. Beckers, E. Peeters, J. J. Apperloo, R. A. J. Janssen, *Chem. Phys. Lett.* **2000**, *328*, 403.
46 P. A. van Hal, R. A. J. Janssen, G. Lanzani, G. Cerullo, M. Zavelani-Rossi, S. De Silvestri, *Phys. Rev. B* **2001**, *64*, 075206.
47 A. Marcos Ramos, M. T. Rispens, J. C. Hummelen, R. A. J. Janssen, *Synth. Met.* **2001**, *119*, 171.
48 J. J. Apperloo, C. Martineau, P. A. van Hal, J. Roncali, R. A. J. Janssen, *J. Phys. Chem. A* **2002**, *106*, 21.
49 A. El-Ghayoury, A. P. H. J. Schenning, P. A. van Hal, C. H. Weidl, J. L. J. van Dongen, R. A. J. Janssen, U. S. Schubert, E. W. Meijer, *Thin Solid Films* **2002**, *403–404*, 97.
50 E. H. A. Beckers, P. A. van Hal, A. P. H. J. Schenning, A. El-Ghayoury, E. Peeters, M. T. Rispens, J. C. Hummelen, E. W. Meijer, R. A. J. Janssen, *J. Mater. Chem.* **2002**, *12*, 2054.
51 A. M. Ramos, S. C. J. Meskers, P. A. van Hal, J. Knol, J. C. Hummelen, R. A. J. Janssen, *J. Phys. Chem. A* **2003**, *107*, 9269.
52 P. A. van Hal, S. C. J. Meskers, R. A. J. Janssen, *Appl. Phys. A* **2004**, *A79*, 41.
53 M. Fujitsuka, T. Makinoshima, O. Ito, Y. Obara, Y. Aso, T. Otsubo, *J. Phys. Chem. B* **2003**, *107*, 739.
54 Y. Obara, K. Takimiya, Y. Aso, T. Otsubo, *Tetrahedron Lett.* **2001**, *42*, 6877.
55 M. J. Frisch, G. W. Trucks, H. B. Schlegel, G. E. Scuseria, M. A. Robb, J. R. Cheeseman, J. A. Montgomery, Jr., T. Vreven, K. N. Kudin, J. C. Burant, J. M. Millam, S. S. Iyengar, J. Tomasi, V. Barone, B. Mennucci, M. Cossi, G. Scalmani, N. Rega, G. A. Petersson, H. Nakatsuji, M. Hada, M. Ehara, K. Toyota, R. Fukuda, J. Hasegawa, M. Ishida, T. Nakajima, Y. Honda, O. Kitao, H. Nakai, M. Klene, X. Li, J. E. Knox, H. P. Hratchian, J. B. Cross, V. Bakken, C. Adamo, J. Jaramillo, R. Gomperts, R. E. Stratmann, O. Yazyev, A. J. Austin, R. Cammi, C. Pomelli, J. W. Ochterski, P. Y. Ayala, K. Morokuma, G. A. Voth, P. Salvador, J. J. Dannenberg, V. G. Zakrzewski, S. Dapprich, A. D. Daniels, M. C. Strain, O. Farkas, D. K. Malick, A. D. Rabuck, K. Raghavachari, J. B. Foresman, J. V. Ortiz, Q. Cui, A. G. Baboul, S. Clifford, J. Cioslowski, B. B. Stefanov, G. Liu, A. Liashenko, P. Piskorz, I. Komaromi, R. L. Martin, D. J. Fox, T. Keith, M. A. Al-Laham, C. Y. Peng, A. Nanayakkara, M. Challacombe, P. M. W. Gill, B. Johnson, W. Chen, M. W. Wong, C. Gonzalez, J. A. Pople, *Gaussian 03, Revision C.02*, Gaussian, Inc., Wallingford CT, **2004**.
56 A. Weller, *Z. Phys. Chem. Neue Folge*, **1982**, *133*, 93.
57 C. Luo, M. Fujitsuka, A. Watanabe, O. Ito, L. Gan, Y. Huang, C.-H. Huang, *J. Chem. Soc., Faraday Trans.* **1998**, *94*, 527.
58 M. Gevaert, P. V. Kamat, *J. Phys. Chem.* **1992**, *96*, 9883.
59 K. Yoshino, S. Nakajima, H. B. Gu, R. Sugimoto, *Jpn. J. Appl. Phys.* **1987**, *26*, L2046.
60 C. Luo, M. Fujitsuka, C.-H. Huang, O. Ito, *J. Phys. Chem. A* **1998**, *102*, 8716.
61 R. A. Marcus, *Annu. Rev. Phys. Chem.* **1964**, *15*, 144.
62 R. A. Marcus, N. Sutin, *Biochim. Biophys. Acta* **1985**, *811*, 265.
63 R. A. Marcus, *Angew. Chem., Int. Ed. Engl.* **1993**, *32*, 1111.
64 H. Heitele, *Angew. Chem., Int. Ed. Engl.* **1993**, *32*, 359.
65 M. L. Horng, J. A. Gardecki, A. Papazyan, M. Maroncelli, *J. Phys. Chem.* **1995**, *99*, 17311.
66 L. Reynolds, J. A. Gardecki, S. J. V. Frankland, M. L. Horng, M. Mroncelli, *J. Phys. Chem.* **1996**, *100*, 10337.